

Stefania Vecchietti, Eleonora Grandi, Stefano Severi, Ilaria Rivolta, Carlo Napolitano, Silvia G. Priori and Silvio Cavalcanti

Am J Physiol Heart Circ Physiol 292:56-65, 2007. First published Sep 15, 2006;
doi:10.1152/ajpheart.00270.2006

You might find this additional information useful...

This article cites 40 articles, 19 of which you can access free at:

<http://ajpheart.physiology.org/cgi/content/full/292/1/H56#BIBL>

This article has been cited by 1 other HighWire hosted article:

Calcium and potassium changes during haemodialysis alter ventricular repolarization duration: in vivo and in silico analysis

S. Severi, E. Grandi, C. Pes, F. Badiali, F. Grandi and A. Santoro
Nephrol. Dial. Transplant., April 1, 2008; 23 (4): 1378-1386.

[\[Abstract\]](#) [\[Full Text\]](#) [\[PDF\]](#)

Updated information and services including high-resolution figures, can be found at:

<http://ajpheart.physiology.org/cgi/content/full/292/1/H56>

Additional material and information about *AJP - Heart and Circulatory Physiology* can be found at:

<http://www.the-aps.org/publications/ajpheart>

This information is current as of November 25, 2009 .

CALL FOR PAPERS | Computational Analyses in Ion Channelopathies

In silico assessment of Y1795C and Y1795H SCN5A mutations: implication for inherited arrhythmogenic syndromes

Stefania Vecchietti,¹ Eleonora Grandi,¹ Stefano Severi,¹ Ilaria Rivolta,²
Carlo Napolitano,² Silvia G. Priori,² and Silvio Cavalcanti¹

¹Cellular and Molecular Engineering Laboratory, Dipartimento di Elettronica, Informatica e Sistemistica, University of Bologna, Cesena; and ²Molecular Cardiology Laboratory, Fondazione Salvatore Maugeri, Istituto di Ricovero e Cura A Carattere Scientifico, Pavia, Italy

Submitted 15 March 2006; accepted in final form 12 September 2006

Vecchietti S, Grandi E, Severi S, Rivolta I, Napolitano C, Priori SG, Cavalcanti S. In silico assessment of Y1795C and Y1795H SCN5A mutations: implication for inherited arrhythmogenic syndromes. *Am J Physiol Heart Circ Physiol* 292: H56–H65, 2007. First published September 15, 2006; doi:10.1152/ajpheart.00270.2006.—The effects of two SCN5A mutations (Y1795C, Y1795H), previously identified in one Long QT syndrome type 3 (LQT3) and one Brugada syndrome (BrS) families, were investigated by means of numerical modeling of ventricular action potential (AP). A Markov model capable of reproducing a wild-type as well as a mutant sodium current (I_{Na}) was identified and was included into the Luo-Rudy ventricular cell model for action potential (AP) simulation. The characteristics of endocardial, mid-myocardial, and epicardial cells were reproduced by differentiating the transient outward current (I_{TO}) and the ratio of slow delayed rectifier potassium (I_{Ks}) to rapid delayed rectifier current (I_{Kr}). Administration of flecainide and mexiletine was simulated by appropriately modifying I_{Na} , calcium current (I_{Ca}), I_{TO} , and I_{Kr} . Y1795C prolonged AP in a rate-dependent manner, and early afterdepolarizations (EADs) appeared during bradycardia in epicardial and midmyocardial cells; flecainide and mexiletine shortened AP and abolished EADs. Y1795H resulted in minimal changes in the APs; flecainide but not mexiletine induced APs heterogeneity across the ventricular wall that accounts for the ST segment elevation induced by flecainide in Y1795H carriers. The AP abnormalities induced by Y1795H and Y1795C can explain the clinically observed surface ECG phenotype. For the first time by modeling the effects of flecainide and mexiletine, we are able to gather mechanistic insights on the response to drugs administration observed in affected patients.

computer modeling; genetics; arrhythmias; sodium channel; antiarrhythmic drugs

CARDIAC SODIUM CHANNEL GENE (*SCN5A*) mutations are associated with at least two inherited arrhythmogenic disorders, Long QT syndrome type 3 (LQT3) and Brugada syndrome (BrS). Both syndromes predispose one to life-threatening ventricular arrhythmias and sudden death that most often occur during sleep or at rest (6, 33, 38). However, they present distinctive ECG phenotypes: the hallmark of LQT3 is the prolongation of QT interval (34, 37), whereas BrS typically shows an ST segment elevation in the right precordial leads, often accompanied by a right bundle branch block (6). The response to class I antiarrhythmic drugs in the two diseases is also remark-

ably different. In BrS, flecainide (6) but not mexiletine (42) allows unmasking an overt phenotype, whereas in LQT3 both mexiletine (32, 36) and flecainide (4, 33) may shorten the QT interval. Functional characterization of mutants has demonstrated that LQT3 is associated with a gain of function mainly caused by a defective current inactivation, whereas BrS mutations produce a loss of function through a variety of different biophysical mechanisms (34). So far, expression studies in heterologous cell lines have provided critical information for the understanding of the biophysical consequences of mutation at the channel-current level, but they have given little insight into the arrhythmogenic mechanisms that initiate and sustain arrhythmias. In the recent years, computer modeling of cardiac excitability has emerged as a most valuable tool to study the effects of mutations on ventricular action potential (AP) (7–9, 48).

Here we report the results of in silico experiments concerning two *SCN5A* mutants that we identified in families with LQT3 (Y1795C) and BrS (Y1795H) (Fig. 1). Extensive in vitro characterization of both allelic variants had been previously carried out (35). The Y1795C mutation exhibited a significantly sustained current when expressed in heterologous cell lines. A small maintained current was also observed in Y1795H. In addition, both mutations caused a significant shift of the inactivation process toward negative potentials. In a previous article (47), a nine-state Markov model was identified to simulate the Na^+ current (I_{Na}) in wild-type (WT) Na^+ cardiac channel and the current alterations observed in Y1795C and Y1795H mutant channels. In this model-based simulation study, we analyzed the mutation-dependent AP shape and duration abnormalities and the effects of mexiletine and flecainide on WT and mutant APs to gather insights on the electrophysiological mechanisms underlying the ECG phenotypes and the responses to these drugs observed in LQT3 and BrS patients.

MATERIALS AND METHODS

Markov model of I_{Na} . The cardiac I_{Na} was modeled by a nine-state Markov chain (Fig. 2) already proposed by Clancy and Rudy (9). The model included three distinct closed states, a conducting open state, and five inactivation states (one fast, two intermediate, and two closed

Address for reprint requests and other correspondence: S. Cavalcanti, DEIS, Viale Risorgimento, 2, I-40136, Bologna, Italy (e-mail: silvio.cavalcanti@unibo.it).

The costs of publication of this article were defrayed in part by the payment of page charges. The article must therefore be hereby marked “advertisement” in accordance with 18 U.S.C. Section 1734 solely to indicate this fact.

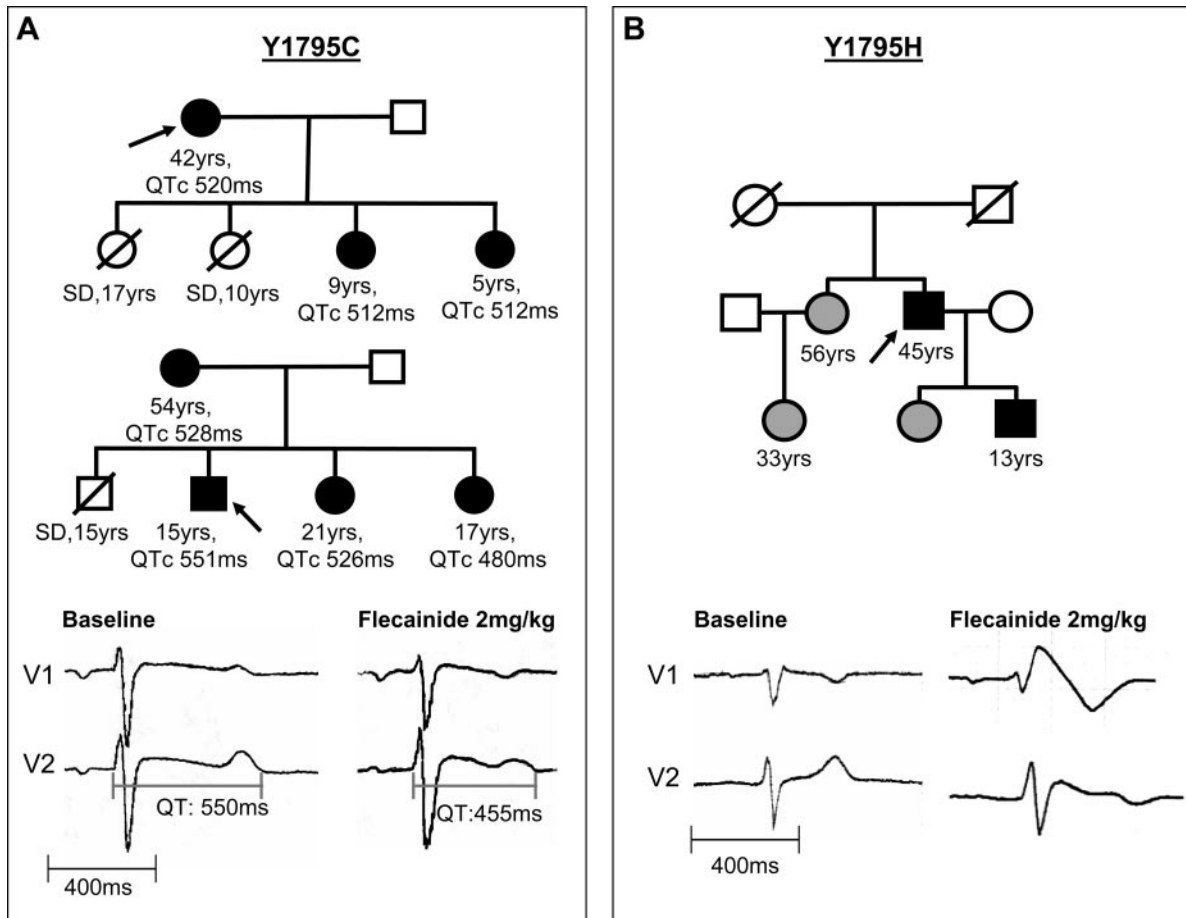


Fig. 1. Pedigrees and representative ECGs of the Y1795C (A) and Y1795H (B) families. Filled symbols represent genetically and clinically affected individuals (black) or silent mutation carriers (grey). The effect of flecainide intravenous administration is depicted at the bottom. QTc (QT interval corrected for heart rate, Bazett's formula) shortening was observed in the Y1795C ECG (from 530 to 470 ms) while 2 mm ST segment elevation was elicited by this drug in Y1795H.

inactivation). The expressions of transition rates are reported in Table 1. The parameters of transition rates were identified as extensively reported in the study by Vecchietti et al. (47) to reproduce by the Markov model the whole cell current measured by Rivolta et al. (35) in WT and mutant channels expressed in HEK-293 cells. The best fit of the current measured by voltage-clamp protocols (activation, inactivation, recovery from inactivation, sustained current, and time to half inactivation) in WT and mutant cells was obtained by assigning

the parameter values listed in Table 2. In particular, the sustained noninactivating component of the I_{Na} characterizing the mutant channels (to a larger extent the Y1795C mutant) was reproduced by significantly altering the transition between the fast inactivation and the intermediate inactivation states with a different assignment of the parameter π in the a_4 transition rate. The agreement between model prediction and electrophysiology curves is shown in the study by Vecchietti et al. (47).

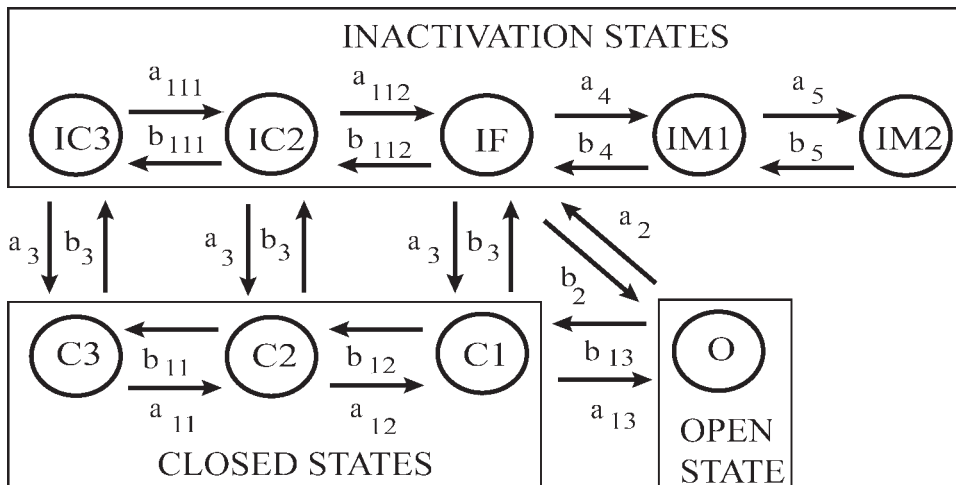


Fig. 2. Diagram of the nine-state Markov model of the cardiac Na^+ current. The model includes three closed states (C1, C2, C3), a conducting open state (O), two closed inactivation states (IC3, IC2), one fast inactivation state (IF), and two intermediate inactivation states (IM1, IM2). The expressions of the transition rates and the assignment of the parameters for WT and mutant channels are reported in Tables 1 and 2.

Table 1. Transition rate expressions

Transition Rates
$a_{11} = [\alpha \exp(-V/17) + \beta \exp(-V/150)]^{-1}$
$a_{12} = [\alpha \exp(-V/15) + \beta \exp(-V/150)]^{-1}$
$a_{13} = [\alpha \exp(-V/12) + \beta \exp(-V/150)]^{-1}$
$b_{11} = \varepsilon \exp(-V/20.3)$
$b_{12} = \zeta \exp(-V/20.3)$
$b_{13} = \eta \exp(-V/20.3)$
$a_{111} = [\theta \exp(-V/17) + \omega \exp(-V/150)]^{-1}$
$a_{112} = [\theta \exp(-V/15) + \omega \exp(-V/150)]^{-1}$
$b_{111} = \varphi \exp(-V/20.3)$
$b_{112} = \kappa \exp(-V/20.3)$
$a_3 = \lambda \exp(-V/\mu)$
$b_3 = \xi (8.4 \times 10^{-3} + 2.0 \times 10^{-5} V)$
$a_2 = (\xi \exp(-V/16.5) + \nu \exp(-V/200))^{-1}$
$b_2 = a_{13} a_2 a_3 / b_{13} b_3$
$a_4 = \pi a_2$
$b_4 = \rho a_3$
$a_5 = \sigma a_2$
$b_5 = \tau \exp(-V/7.7)$

Values are expressed in ms^{-1} .

To reproduce the heart rate dependence of the maintained I_{Na} for Y1795C shown in the Rivolta et al. study (35), two distinct sets of parameters were identified (Table 2): one for bradycardia (40 beats/min) and one for tachycardia (115 beats/min). Both sets reproduce the voltage-clamp curves pretty well. The parameters for the 70 beats/min condition were assigned as the weighted-average between the values at 40 and 115 beats/min.

Ventricular cell computer model. The ventricular AP simulator was based on the Luo-Rudy (LRd) model (13) (Fig. 3) that was implemented in Simulink 5 (The MathWorks, Natick, MA). Intra- and extracellular ion concentrations were set to constant values (extracellular $[\text{K}^+] = 4.5 \text{ mmol/l}$, intracellular $[\text{K}^+] = 141.2 \text{ mmol/l}$, extracellular $[\text{Na}^+] = 140 \text{ mmol/l}$, intracellular $[\text{Na}^+] = 10 \text{ mmol/l}$ and extracellular $[\text{Ca}^{2+}]_e = 1.2 \text{ mmol/l}$), except for intracellular $[\text{Ca}^{2+}]$ for which dynamic changes were simulated. The transient outward current (I_{TO}) was modeled according to Dumaine et al. (12). The original formulation of the I_{Na} was replaced with the nine-state Markov model. To reproduce the heterozygous condition of Y1795C and Y1795H patients, 50% mutant and 50% WT channels were simulated. The maximum Na^+ conductance (G_{Na}) was set to 16 $\text{mS}/\mu\text{F}$ for WT, in agreement with Faber and Rudy (13). G_{Na} was set to 29.46 $\text{mS}/\mu\text{F}$ for Y1795C and 5.96 $\text{mS}/\mu\text{F}$ for Y1795H to account for the experimentally measured ratios (mutants vs. WT) of I_{Na} peaks (35). All the kinetic rates were normalized to 37°C with a Q10 of 2.1 (5, 40).

Transmural heterogeneity (23, 43) (epicardium, endocardium, and midmyocardium cells) of the AP was modeled by setting the I_{TO} expression level (9) and the density ratio between slow and rapid components of the delayed-rectifier potassium current ($I_{\text{Ks}}/I_{\text{Kr}}$) (22). In epicardial (Epi) cells the maximal I_{TO} conductance (G_{TO}) was set to 1.1 $\text{mS}/\mu\text{F}$ and the $I_{\text{Ks}}/I_{\text{Kr}}$ was set to 63. In midmyocardial (M) cells, G_{TO} was set to 0.5 $\text{mS}/\mu\text{F}$ and $I_{\text{Ks}}/I_{\text{Kr}}$ was set to 23.3. In endocardial (Endo) cells, G_{TO} was set to 0.05 $\text{mS}/\mu\text{F}$ and $I_{\text{Ks}}/I_{\text{Kr}}$ was set to 29.6. This setting allowed a numerical reconstruction of Epi, M, and Endo cells APs. The maximum conductance of the L-type calcium current was decreased by 20% with respect to the original LRd formulation in all cells (3) in accordance with Ref. 12.

Pacing was simulated by a 1-ms pulse train of 50 A/F in amplitude with frequency of 40, 70, and 115 beats/min. Rosenbrock variable-step algorithm (max step 10 μs) was used to numerically solve the model equations (41). To ensure a steady-state condition, 180-s long simulations were performed; all the data shown refer to the last beat. AP duration (APD) was measured at 90% of repolarization (APD₉₀).

Flecainide and mexiletine simulation. The blocking effects of flecainide and mexiletine were mimicked by reducing the maximal conductance of I_{Na} , I_{Ca} , I_{TO} , and I_{Kr} (Table 3).

According to our experimental data (not shown), flecainide induces mild negative shift of the availability curve of I_{Na} (WT: 3 mV, Y1795C: 7 mV, Y1795H: 8 mV). The parameter assignment for the kinetic rate a_3 in the Markov model was modified accordingly (see Table 4).

RESULTS

Simulated WT AP. When the WT I_{Na} Markov model was included in the ventricular cell model, the simulated APs shape resembled the typical reported waveforms (2) for the three cell types (Fig. 4, left). The APDs at 70 beats/min were the following: Endo, 162 ms; Epi, 157 ms; M, 181 ms. The APDs at 40 and 115 beats/min are reported in Table 5. AP morphology did not vary with changes in pacing frequency (40 beats/min up to 115 beats/min).

Effects of Y1795C mutation on APs. The simulated Y1795C APs were longer compared with those of the WT in all cell layers (Endo: 6%, Epi: 10%, M: 16% at a pacing rate of 70 beats/min) and showed remarkable increase of the AP prolongation when heart rate decreases (Fig. 4 and Table 5). This effect was more prominent in Epi and in M cells, in which early afterdepolarizations (EADs) appeared at 40 beats/min (Fig. 4, middle).

Effects of Y1795H mutation on AP. The heterozygous condition for the Y1795H mutant channel only slightly changed the AP morphology (Fig. 4, right) and duration (Table 5) with respect to the WT. Albeit in vitro characterization shows that Y1795H induces a small sustained I_{Na} (35), the resulting AP prolongation was negligible in all cell types (Endo: 1.2%, Epi: 1.5%, M: 1.7% at a pacing rate of 70 beats/min). The reduced current availability of the Y1795H channel resulted in a mild reduction of the AP upstroke amplitude (10% in Epi cell) compared with the WT.

Effects of flecainide and mexiletine on the WT AP. The in silico simulation of flecainide induced transmural opposite responses in WT APDs (Table 5). At 40 beats/min, 13%

Table 2. Na channel model parameters for wild-type and mutant channels

Parameters	Y1795H	Wild Type	Y1795C	
			40 beats/min	115 beats/min
α	0.0141	0.0378	0.0077	0.0196
β	0.0345	0.0925	0.2663	0.168
ε	0.5751	0.2492	0.3962	0.4409
ζ	0.7676	0.3326	0.5287	0.5885
η	1.0801	0.4681	0.7442	0.8281
θ	0.0313	0.1093	0.0240	0.0435
ω	0.0558	0.1949	0.7617	0.3684
φ	0.5751	0.1917	0.1278	0.4409
κ	0.7676	0.2559	0.1705	0.5885
λ	1.1380×10^{-6}	3.7933×10^{-7}	4.0000×10^{-7}	13.800×10^{-7}
μ	7.6029	6.1839	7.1839	7.1839
ν	3.0000	1.0000	0.6667	2.3000
ξ	0.0133	0.0159	4.0661×10^{-6}	0.0024
ν	0.0607	0.0722	0.1275	0.0676
π	4.8000×10^{-4}	0.0022	0.0001	0.0009
ρ	0.2400	0.1000	0.1125	0.1000
σ	0.1737×10^{-4}	0.0924×10^{-4}	0.0024×10^{-4}	0.1053×10^{-4}
τ	0.4097×10^{-7}	0.0854×10^{-7}	0.0004×10^{-7}	0.1133×10^{-7}

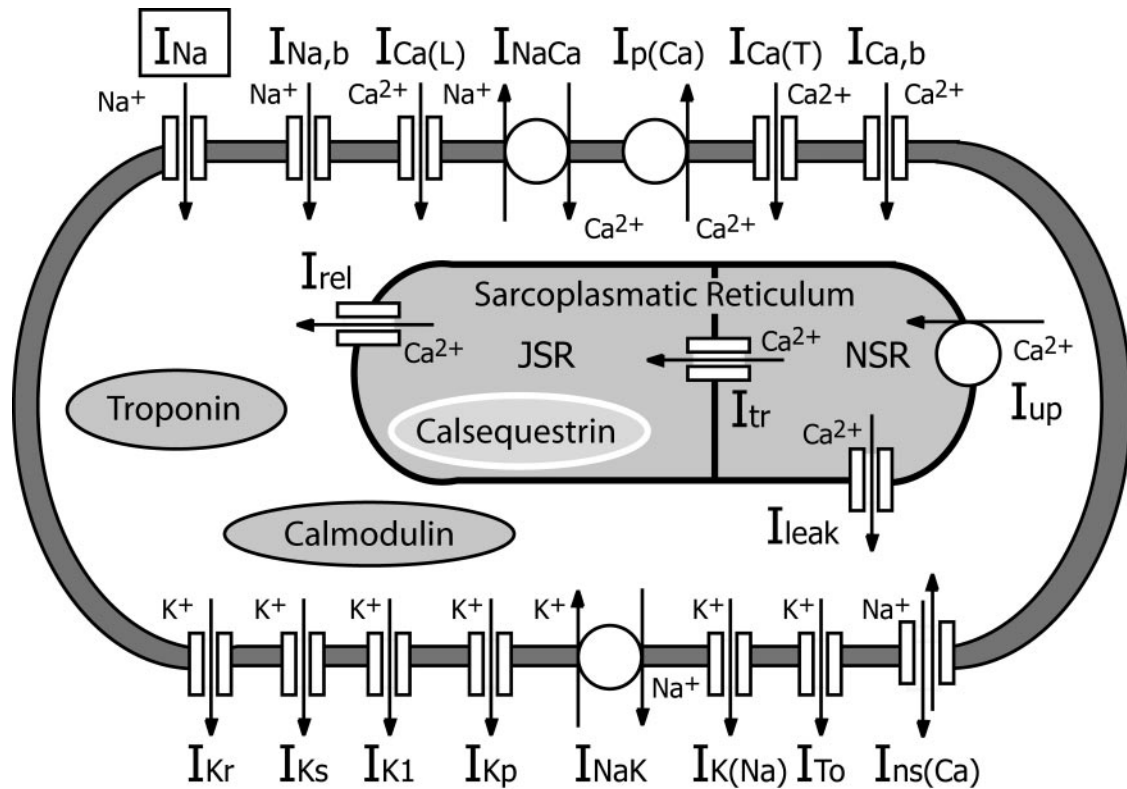


Fig. 3. Schematic diagram of the Luo-Rudy ventricular cell model, in which the Markov model of the Na⁺ current (*I_{Na}*) was inserted. Detailed explanation of symbols can be found in Ref. 13.

prolongation of the APD₉₀ in Epi and 11% shortening of APD₉₀ in Endo was forecast. This finding is in agreement with other experimental results (21). Mexiletine slightly shortened APD₉₀ (Table 5) in both Epi and Endo cells (Epi: 2%, Endo: 6%, at 40 beats/min). Both drugs caused an AP shortening in M cells (flecainide: 15%, mexiletine: 10%, at 40 beats/min).

Effects of flecainide and mexiletine on the Y1795C AP. In bradycardia, flecainide and mexiletine caused APD₉₀ to shorten in the Y1795C mutant cell but with a stronger effect in the case of flecainide (Table 5): -22.5% vs. -13.5% in Endo cells at 40 beats/min. Notably, both drugs inhibit the onset of EADs in Epi and M cells (Fig. 5). As already shown for WT, at 115 beats/min flecainide caused the lengthening of APD in the Epi cells (see Table 5).

Effects of flecainide and mexiletine on the Y1795H AP. Flecainide also elicited a myocardial layer-specific response in the case of Y1795H mutant (Fig. 6, left). Flecainide reduced

APD in Endo and M cells (Table 5); in the Epi cells a striking complete loss of the AP dome occurred at 40 beats/min (APD₉₀: from 166 to 116 ms), whereas at 115 beats/min an alternating pattern appeared. Conversely, mexiletine caused modest AP changes (Fig. 6, right, and Table 5) with APD decreasing in M and Endo cells and increasing in Epi cells.

Interestingly, the effect of flecainide on AP morphology of the Epi cell was dependent on the amount of *I_{Na}* blockade (Fig. 7). For a 40% block, domeless APs alternatively separated by long APs were predicted (Fig. 7, middle). The oscillatory pattern was stable over time. For a 30% current reduction, oscillations in the APD disappeared, and a stable pattern of long markedly notched APs was reproduced (Fig. 7, bottom). Similar transitions through different AP waveforms were observed when the pacing frequency was raised up to 115 beats/min by maintaining the 50% of *I_{Na}* blockade (Table 5).

Since the different response elicited by flecainide and mexiletine on the Epi cell AP (Fig. 6) was obtained by simulating the

Table 3. Percentage of current blocking used to mimic flecainide and mexiletine administration

Current	Blocking, %	
	Flecainide	Mexiletine
<i>I_{Na}</i>	50 (24)	50 (19)
<i>I_{Ca}</i>	45 (17, 18)	25 (26, 30)
<i>I_{TO}</i>	10 (1, 44)	
<i>I_{Kr}</i>	10 (15, 31, 49)	

I_{Na}, sodium current; *I_{Ca}*, calcium current; *I_{TO}*, transient outward current; *I_{Kr}*, rapid delayed rectifier potassium current. Bibliographic references are indicated in parentheses.

Table 4. Parameter assignment for kinetic rate *a₃* in Markov model

	λ
Wild type	7.021×10^{-8}
Y1795C	
40 beats/min	1.388×10^{-8}
115 beats/min	2.916×10^{-8}
Y1795H	1.112×10^{-8}

Modification of the parameters of kinetic rate $a_3 = \lambda \exp(-V/\mu)$ to reproduce negative shift of availability curve induced by flecainide (10 μ M). The parameter μ was set to 6.0773 in all cases.

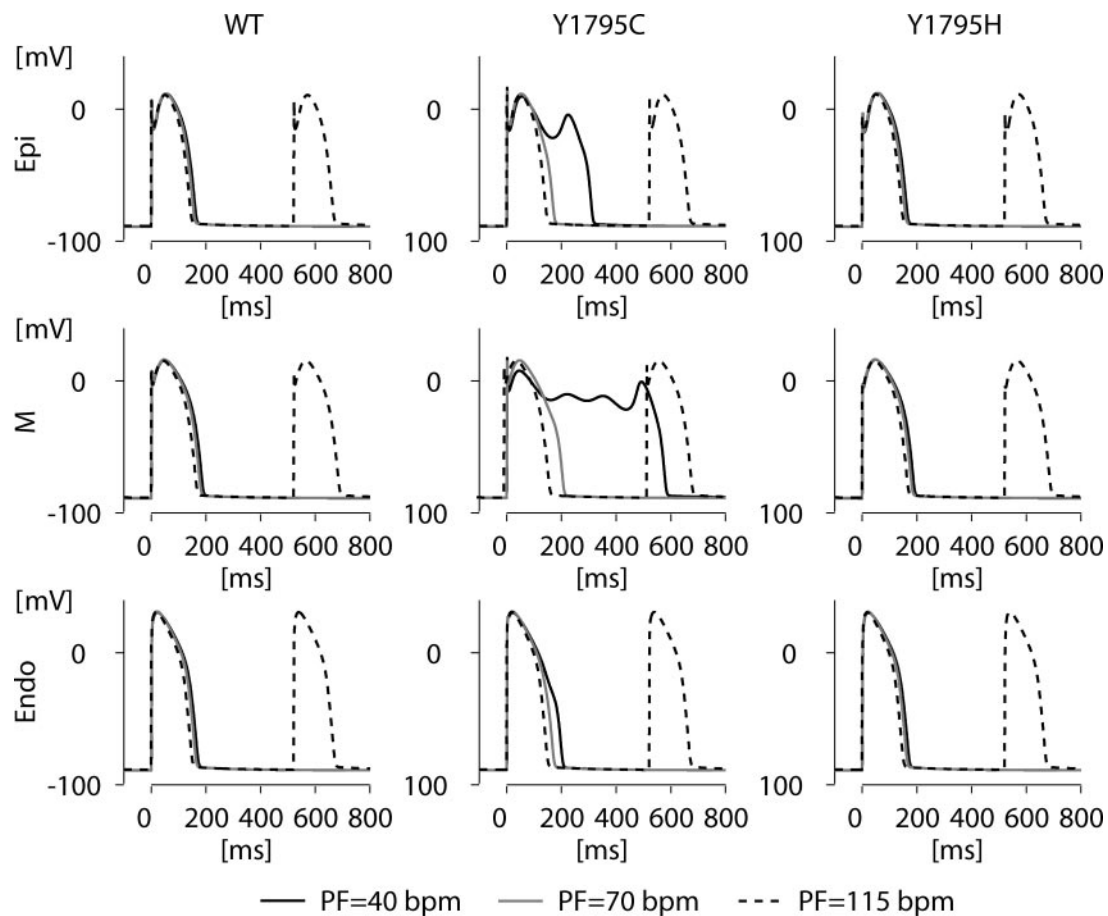


Fig. 4. Y1795C mutation (*middle*) affects action potential (AP) of the three cells composing the ventricular wall [Epi, epicardial; M, midmyocardial; Endo, endocardial] in a rate-dependent manner. The major effect is shown at the pacing frequency (PF) of 40 beats/min when early afterdepolarizations (EADs) appear in Epi and M cell AP. Y1795H mutation (*right*) does not have remarkable effects on the AP of the three myocardial layers.

same (50%) I_{Na} reduction for the two drugs, the simultaneous different block of the other ion currents (Table 3) seems to take part in differentiating drug-induced AP alterations. To investigate the role of each current, we analyzed the AP sensitivity to different levels of I_{Ca} , I_{TO} , and I_{Kr} block (Fig. 8). The loss of the AP dome in Epi cells, characterizing the flecainide simulation (Fig. 8, BL1 curve), also persisted when I_{Kr} was either completely blocked (data not shown) or not blocked at all (Fig. 8, BL2 curve). If I_{Kr} and I_{TO} were not blocked (Fig. 8, BL3 curve), the APD was further reduced. The AP was still domeless when the I_{Ca} blockade was reduced from 45% to 35% (Fig. 8, BL4 curve). With 35% block of I_{Ca} , the superimposition of a low level of I_{TO} block (10%) caused the appearance of the AP dome with a markedly pronounced notch (Fig. 8, BL5 curve). Without the blockade of I_{Kr} and I_{TO} , the restoration of the AP morphology with dome occurred when a 25% I_{Ca} blockade was simulated (Fig. 8, BL6 curve). The last condition corresponds to the simulation of mexiletine. Notably, the abrupt changes in AP morphology with respect to the degree of block enlightens on the “all or none” nature of this phenomenon.

DISCUSSION

In the present study, we investigated with numerical experiments the effect of two mutations of residue 1795 (Y1795C and Y1795H) of the cardiac sodium channel protein that cause

LQT3 and BrS, respectively. We previously reported the heterologous expression of both mutants, and we demonstrated that they modify the biophysical properties of the I_{Na} (35). Specifically, Y1795C leads to a residual-sustained inward I_{Na} that is consistent with the LQT3 phenotype, whereas Y1795H accelerates inactivation thus reducing current availability.

Here we numerically reproduced the biophysical properties of WT and mutant sodium channels by a Markov model of I_{Na} , and we implemented these data in the Lrd ventricular AP model (12, 13) to assess: 1) the mutation-dependent AP abnormalities in Epi, Endo, and M cells and 2) the response to sodium channel-blocking drugs known to modify the ECG in LQT3 and BrS patients. On the basis of such analyses, we show how the mutation-dependent AP alterations account for the patients' electrocardiographic phenotype and provide clues for the understanding of arrhythmogenic mechanisms associated with these mutations.

Effects of Y1795C and Y1795H on AP in the three myocardial layers. We took advantage from previously published data (43) to simulate the transmural heterogeneity of the AP by modulating the amount of the I_{TO} and the ratio between I_{Ks} and I_{Kr} components (9, 22, 23). We then characterized the alterations induced by each of the mutants on the AP of Epi, Endo, and M cells at different pacing rates.

Table 5. APD₉₀ values in the different cell types with and without drugs resulting from simulations with the pacing rate of 40 115 beats/min.

	40 beats/min			115 beats/min		
	Epi	M	Endo	Epi	M	Endo
No drug						
WT	161	185	167	146	163	148
LQTS	EADs	EADs	201	150	167	150
BrS	166	187	170	151	169	151
Flecainide						
WT	182	157	149	168	155	141
LQTS	180	165	156	187	155	141
BrS	116	165	156	*	158	144
Mexiletine						
WT	158	167	157	146	158	144
LQTS	180	205	174	147	158	143
BrS	168	172	168	153	159	145

Values are expressed in milliseconds. Epi, epicardial; M, myocardial; Endo, endocardial; WT, wild type; LQTS, Long QT syndrome; BrS, Brugada syndrome; APD₉₀, 90% repolarization of action potential (AP) duration. *Alternating pattern: a long epicardial AP (APD₉₀ = 227 ms) was followed by two shorter activations (loss of dome) of different duration (97 and 125 ms), and by another long-short AP sequence (APD₉₀ = 225 ms and APD₉₀ = 97 ms).

Numerical simulation confirmed the observation made by Clancy et al. (10) in their model of Endo cells that bradycardia accentuates the APD prolongation as a consequence of an increased sustained I_{Na} at slower rates (Fig. 4). In addition, we

showed that the effect of the late I_{Na} during bradycardia was more pronounced in Epi and M cells than in Endo cells. Whereas Y1795C only induced APD prolongation in the Endo cell model (10), in the Epi and M cell models, the mutation also induced EADs (Fig. 4, middle). In Epi cells, EADs developed despite a shorter basal AP in this cell type with respect to Endo cells. This is due to the presence of a larger I_{TO} in this layer. The prominent notch in AP phase 1 of the Epi cells, due to I_{TO} , determines a different balance of currents in the subsequent phases of the AP, allowing the sustained I_{Na} to trigger EADs. In fact, we did not find EADs by simulating Y1795C Epi cells with $G_{TO} = 50$ S/F (as Endo cell, data not shown). These results are in agreement with the LQT3 phenotype observed in the Y1795C carriers and with the fact that three life-threatening events (three sudden deaths and one cardiac arrest) occurred during sleep (Fig. 1).

At variance with Y1795C, the Y1795H mutation induced only negligible changes of AP morphology in the three myocardial layers, in agreement with the clinical findings that the BrS phenotype observed in the carriers of the mutation was only evident upon pharmacological challenge with flecainide (Fig. 1).

Response of mutants to sodium channel blockers. The Y1795C model displayed a reduction of Endo APD by 22% with flecainide and by 13% with mexiletine. Interestingly, in the clinical setting, flecainide administration (2 mg/kg) reduced

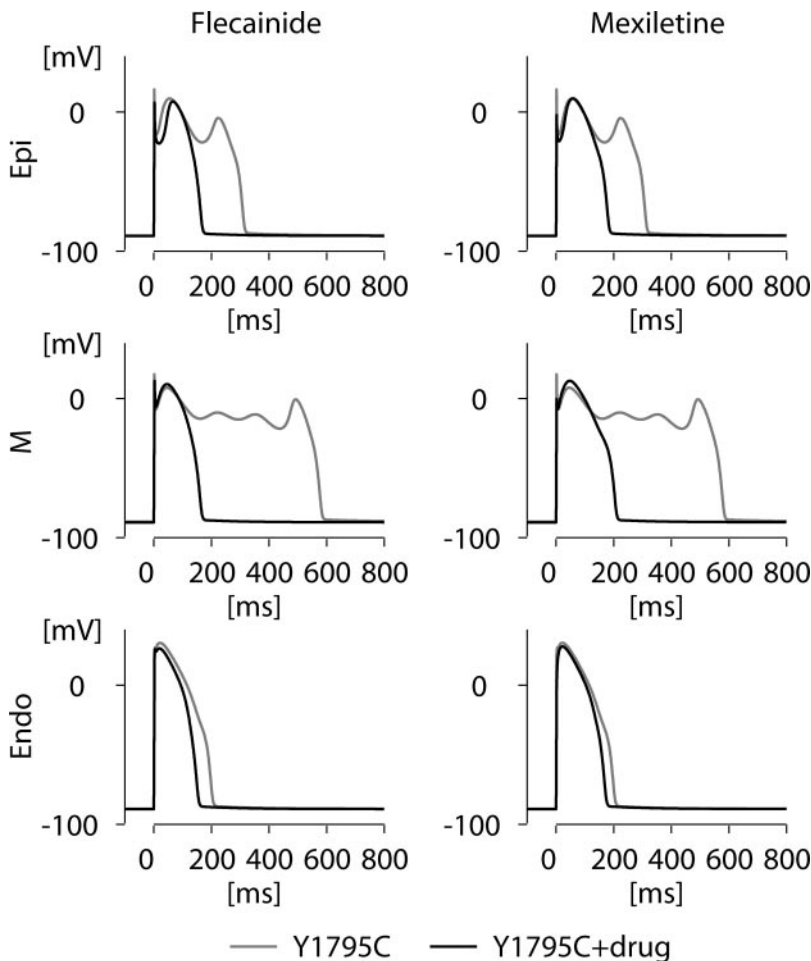


Fig. 5. Effect of flecainide (left) and mexiletine (right) on ventricular cell AP in presence of Y1795C mutation at the pacing rate of 40 beats/min. Both drugs reduce AP duration in Endo cell and suppress EADs in Epi and M cells.

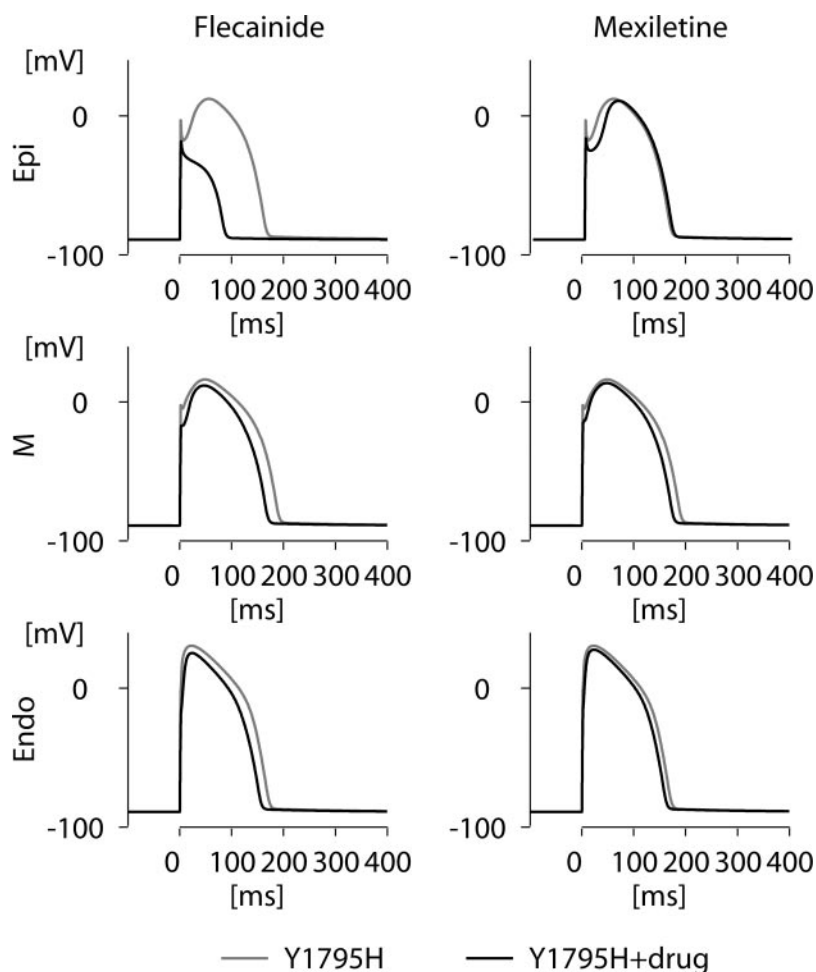


Fig. 6. Effect of flecainide (*left*) and mexiletine (*right*) on ventricular cell AP in presence of Y1795H mutation at the pacing rate of 40 beats/min. Flecainide but not mexiletine causes the appearance of a domeless AP in Epi cells.

the QT interval to the same extent (4, 32) (Fig. 1). These data are consistent with that shown in LQT3 patients in whom class I antiarrhythmic drugs clearly shortened the QT interval (36). In our simulations, both drugs suppressed the EADs in M and Epi cells. The efficacy of the two drugs in suppressing EADs is consistent with the observation made in a mouse model of LQT3 (46) and provides a mechanistic explanation for the prevention of lethal arrhythmias observed over a 5-year follow up in a 5-year-old LQT3 patient who experienced a cardiac arrest while on β -blocker therapy but was subsequently protected by mexiletine treatment (39).

The simulation of flecainide administration in the case of Y1795H experiments induced shortening of the APD in Endo and in M cells, whereas in Epi cells, AP alterations of both duration and morphology were observed (see Fig. 6, *left*, and Fig. 7). The beat-to-beat AP alteration shown in Fig. 7 (*middle*) could be the cellular counterpart of T wave alternans (TWA) (28). In fact, TWA have been reported in BrS patients upon class Ic drug administration (29), and they may be a marker of electrical instability (27). Thus our finding supports the proarrhythmic potential of class Ic drug administration in BrS patients.

In the Epi cells the AP showed a loss of the AP dome: this phenomenon has been suggested as the substrate for the ST segment elevation observed in BrS. Accordingly, our *in silico* analysis predicts that carriers of the Y1795H mutation would

have minimal ECG changes at baseline but would respond to flecainide with a prominent ST segment elevation and electrical instability. Once again this is in agreement with the clinical findings showing a "coved-type" ST segment elevation only after flecainide administration (Fig. 1). Yan and Antzelevitch (50) suggested that the strong I_{TO} current of epicardial cells in the presence of a reduced inward current is responsible for the loss of AP dome. Coherently with this hypothesis we observed prompt AP morphology normalization when I_{TO} was decreased by 50%. At variance with flecainide, mexiletine induced only a slight APD reduction with no loss of the AP dome. This is in agreement with clinical observations by Shimizu et al. (42), who showed that mexiletine did not elicit ST segment elevation in BrS patients.

As of today, a conclusive explanation of the differential effect of flecainide and mexiletine in the BrS patients is not available. Our data suggest that flecainide, but not mexiletine, unmasked BrS silent mutation mainly because of their differential blocking effect on the inward current (greater extent the I_{Ca} block). Thus we suggest that in presence of sodium channel blockers, the balance between I_{Ca} and I_{TO} has to be crucially important for unmasking the arrhythmogenic substrate in BrS patients. This hypothesis is in accordance with the experimental findings of Fish and Antzelevitch (14), whose data suggested that combined calcium channel block may be more effective than sodium channel block alone in unmasking the

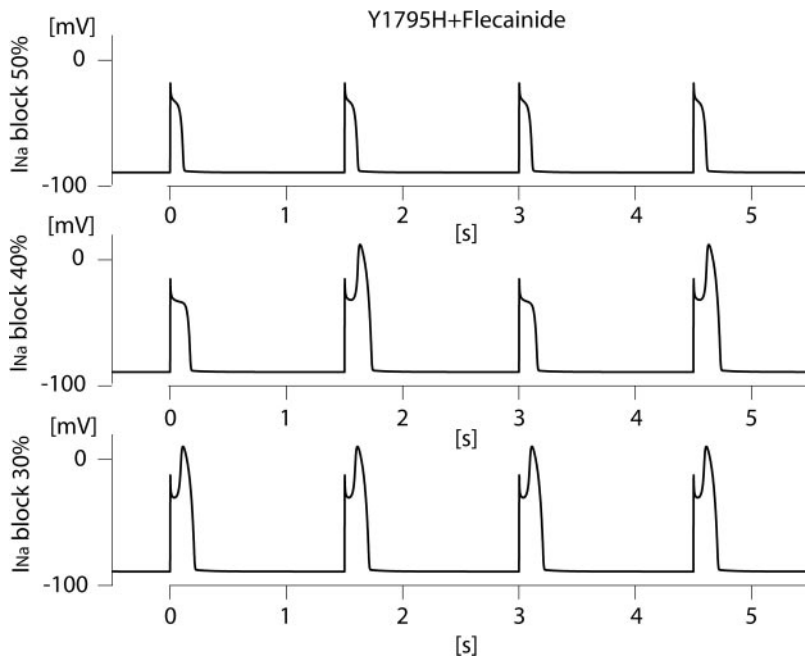


Fig. 7. AP morphology changes due to different levels of flecainide-induced I_{Na} blockade in Epi cell in presence of Y1795H mutation. At a blocking level of 40%, an alternation of prolonged and domeless AP appeared; the AP dome was stably restored at 30% I_{Na} reduction.

BrS and that pharmacological agents that inhibit I_{TO} may be useful in preventing arrhythmias in BrS patients.

Study limitations. We used a computer model based on the well-established LRd model that has been already used to assess the impact of mutations on AP in patients with inherited arrhythmogenic disorders (7–9, 16). Qualities and limitations of this model, which is mostly based on guinea pig experimental data, have been extensively discussed (7, 25, 45). It is worth to note that for the present analysis, we considered as control the APs computed by model with the WT human cardiac Na channel, and we focused on the impact of mutations on the AP with respect to this condition. Thus the dependence of the results from the model setting should be limited. Nevertheless, models of human ventricular cells recently published (20, 45) should be used in further investigations.

The present simulation analysis assumes the existence of transmural heterogeneity of repolarization to an extent similar to that observed in animal studies (2). It is fair to note that the role of transmural dispersion of repolarization in the human heart is still under debate (11). Our simulation results support

the hypothesis that transmural heterogeneity can play a crucial role in the ECG phenotype of I_{Na} mutations.

We did not consider the rate-dependent Na channel binding properties of flecainide and mexiletine. In fact, the recovery from drug block is rapid with mexiletine and slow for flecainide. Liu et al. (24) showed a 10% increase of flecainide-induced blocking when pacing rate was changed in a physiological range from 1 to 2 Hz. A lower variation of the blocking degree is expected for mexiletine. Despite the variations of drug blocking due to heart rate changes are modest, they could influence AP morphology and duration.

The assignment of current blocking is not without uncertainties because of the lack of consistent experimental data assessing the effects of the two drugs. However, the sensitivity analysis reported in Fig. 8 makes the assignment less critical demonstrating that the loss of AP dome kept on also when limited block extents were tested.

In conclusion, in this study we investigated by computer simulation the effects of two SCN5A mutations on the AP of Endo, Epi, and M cells, and we mimicked their response to

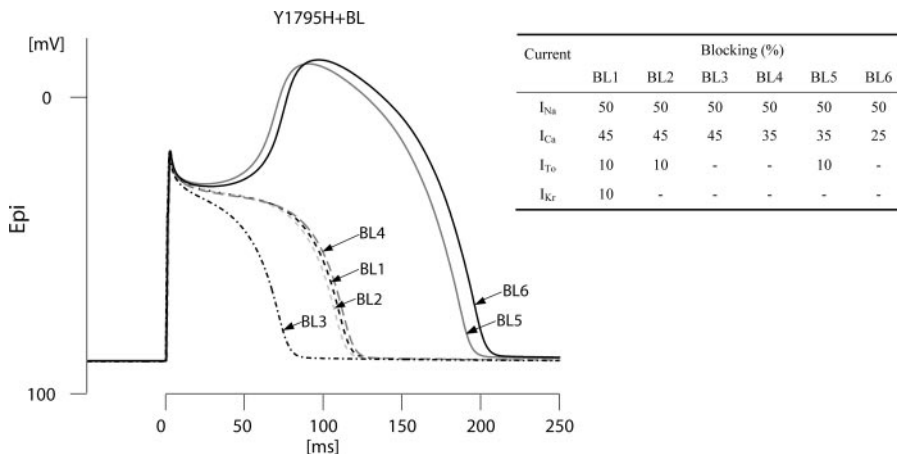


Fig. 8. AP morphology changes induced by different levels of I_{Na} , calcium current (I_{Ca}), transient outward current (I_{TO}), and rapid delayed rectifier potassium current (I_{Kr}) blocking in presence of Y1795H mutation (Epi cell, 40 beats/min).

flecainide and mexiletine. We demonstrate that there is a remarkable agreement between the cellular abnormalities and the electrocardiographic manifestations observed in the carriers of the two genetic defects. Furthermore, we show that a “gain of function” mutation of SCN5A induces bradycardia-dependent APD prolongation in Epi and M cells leading to development of EADs. In this framework, both mexiletine and flecainide reverse the APD prolongation and prevent the EADs. This effect is likely to be a direct consequence of the blockade of the late I_{Na} . Interestingly, our data show for the first time that a loss of function SCN5A mutation may induce only minimal effect on the shape of the APD across the myocardium and is therefore consistent with a normal ECG. It is only in the presence of selective perturbation of other currents that it is possible to reveal such a concealed arrhythmogenic syndrome. This evidence accounts for the variability of the ST segment elevation at ECG and for the paroxysmal nature of the arrhythmic events in Brugada Syndrome.

GRANTS

This study was supported by Ricerca Finalizzata 2003/180, Fondo per gli Investimenti della ricerca di Base RBNE01XMP4_006.

REFERENCES

- Akar FG, Wu RC, Deschenes I, Aroundas AA, Piacentino V, III, Houser SR, Tomaselli GF. Phenotypic differences in transient outward K^+ current of human and canine ventricular myocytes: insights into molecular composition of ventricular I_{to} . *Am J Physiol Heart Circ Physiol* 286: H602–H609, 2004.
- Antzelevitch C, Fish J. Electrical heterogeneity within the ventricular wall. *Basic Res Cardiol* 96: 517–527, 2001.
- Banyasz T, Fulop L, Magyar J, Szentandrassy N, Varro A, Nanasi PP. Endocardial versus epicardial differences in L-type calcium current in canine ventricular myocytes studied by action potential voltage clamp. *Cardiovasc Res* 58: 66–75, 2003.
- Benhorin J, Taub R, Goldmit M, Kerem B, Kass RS, Windman I, Medina A. Effects of flecainide in patients with new SCN5A mutation: mutation-specific therapy for long-QT syndrome? *Circulation* 101: 1698–1706, 2000.
- Benndorf K, Nilius B. Inactivation of sodium channels in isolated myocardial mouse cells. *Eur Biophys J* 15: 117–127, 1987.
- Brugada P, Brugada J. Right bundle branch block, persistent ST segment elevation and sudden cardiac death: a distinct clinical and electrocardiographic syndrome. A multicenter report. *J Am Coll Cardiol* 15: 1391–1396, 1992.
- Clancy CE, Rudy Y. Linking a genetic defect to its cellular phenotype in a cardiac arrhythmia. *Nature* 400: 566–569, 1999.
- Clancy CE, Rudy Y. Cellular consequences of HERG mutations in the long QT syndrome: precursors to sudden cardiac death. *Cardiovasc Res* 50: 301–313, 2001.
- Clancy CE, Rudy Y. Na^+ channel mutation that causes both Brugada and long-QT syndrome phenotypes: a simulation study of mechanism. *Circulation* 105: 1208–1213, 2002.
- Clancy CE, Tateyama M, Kass RS. Insights into the molecular mechanisms of bradycardia-triggered arrhythmias in long QT-3 syndrome. *J Clin Invest* 110: 1251–1262, 2002.
- Drouin E, Charpentier F, Gauthier C, Laurent K, Le M. Electrophysiological characteristics of cells spanning the left ventricular wall of human heart: evidence for presence of M cells. *J Am Coll Cardiol* 26: 185–192, 1995.
- Dumaine R, Towbin JA, Brugada P, Vatta M, Nesterenko DV, Nesterenko VV, Brugada J, Brugada R, Antzelevitch C. Ionic mechanisms responsible for the electrocardiographic phenotype of the Brugada syndrome are temperature dependent. *Circ Res* 85: 803–809, 1999.
- Faber GM, Rudy Y. Action potential and contractility changes in $[Na^+]_i$ overloaded cardiac myocytes: a simulation study. *Biophys J* 78: 2392–2404, 2000.
- Fish JM, Antzelevitch C. Role of sodium and calcium channel block in unmasking the Brugada syndrome. *Heart Rhythm* 1: 210–217, 2004.
- Follmer CH, Cullinan CA, Colatsky TJ. Differential block of cardiac delayed rectifier current by class Ic antiarrhythmic drugs: evidence for open channel block and unblock. *Cardiovasc Res* 26: 1121–1130, 1992.
- Gima K, Rudy Y. Ionic current basis of electrocardiographic waveforms: a model study. *Circ Res* 90: 889–896, 2002.
- Hancox JC, Convery M. Inhibition of L-type calcium current by flecainide in isolated single rabbit atrioventricular nodal myocytes. *Experimental Clin Cardiol* 2: 163–170, 1997.
- Hatem S, Le G, Le H, Couetil JP, Deroubaix E. Differential effects of quinidine and flecainide on plateau duration of human atrial action potential. *Basic Res Cardiol* 87: 600–609, 1992.
- Hering S, Bodewei R, Wollenberger A. Sodium current in freshly isolated and in cultured single rat myocardial cells: frequency and voltage-dependent block by mexiletine. *J Mol Cell Cardiol* 15: 431–444, 1983.
- Iyer V, Mazhari R, Winslow RL. A computational model of the human left-ventricular epicardial myocyte. *Biophys J* 87: 1507–1525, 2004.
- Krishnan SC, Antzelevitch C. Sodium channel block produces opposite electrophysiological effects in canine ventricular epicardium and endocardium. *Circ Res* 69: 277–291, 1991.
- Liu DW, Antzelevitch C. Characteristics of the delayed rectifier current (IKr and IKs) in canine ventricular epicardial, midmyocardial, and endocardial myocytes. A weaker IKs contributes to the longer action potential of the M cell. *Circ Res* 76: 351–365, 1995.
- Liu H, Gintant GA, Antzelevitch C. Ionic bases for electrophysiological distinctions among epicardial, midmyocardial, and endocardial myocytes from the free wall of the canine left ventricle. *Circ Res* 72: 671–687, 1993.
- Liu H, Tateyama M, Clancy CE, Abriel H, Kass RS. Channel openings are necessary but not sufficient for use-dependent block of cardiac Na^+ channels by flecainide: evidence from the analysis of disease-linked mutations. *J Gen Physiol* 120: 39–51, 2002.
- Luo CH, Rudy Y. A dynamic model of the cardiac ventricular action potential. I. Simulations of ionic currents and concentration changes. *Circ Res* 74: 1071–1096, 1994.
- Mitcheson JS, Hancox JC. Modulation by mexiletine of action potentials, L-type Ca current and delayed rectifier K current recorded from isolated rabbit atrioventricular nodal myocytes. *Pflügers Arch* 434: 855–858, 1997.
- Morita H, Nagase S, Kusano K, Ohe T. Spontaneous T wave alternans and premature ventricular contractions during febrile illness in a patient with Brugada syndrome. *J Cardiovasc Electrophysiol* 13: 816–818, 2002.
- Morita H, Zipes DP, Lopshire J, Morita ST, Wu J. T wave alternans in an in vitro canine tissue model of Brugada syndrome. *Am J Physiol Heart Circ Physiol* 291: H421–H428, 2006.
- Ohkubo K, Watanabe I, Okumura Y, Yamada T, Masaki R, Kofune T, Oshikawa N, Kasamaki Y, Saito S, Ozawa Y, Kanmatsuse K. Intravenous administration of class I antiarrhythmic drug induced T wave alternans in an asymptomatic Brugada syndrome patient. *Pacing Clin Electrophysiol* 26: 1900–1903, 2003.
- Ono K, Kiyosue T, Arita M. Comparison of the inhibitory effects of mexiletine and lidocaine on the calcium current of single ventricular cells. *Life Sci* 39: 1465–1470, 1986.
- Paul AA, Witchel HJ, Hancox JC. Inhibition of the current of heterologously expressed HERG potassium channels by flecainide and comparison with quinidine, propafenone and lignocaine. *Br J Pharmacol* 136: 717–729, 2002.
- Priori SG, Napolitano C, Cantu F, Brown AM, Schwartz PJ. Differential response to Na^+ channel blockade, beta-adrenergic stimulation, and rapid pacing in a cellular model mimicking the SCN5A and HERG defects present in the long-QT syndrome. *Circ Res* 78: 1009–1015, 1996.
- Priori SG, Napolitano C, Schwartz PJ, Bloise R, Crotti L, Ronchetti E. The elusive link between LQT3 and Brugada syndrome: the role of flecainide challenge. *Circulation* 102: 945–947, 2000.
- Priori SG, Rivolta I, Napolitano C. Genetics of long QT, Brugada and other channelopathies. In: *Cardiac Electrophysiology* (4th ed.), edited by Zipes DP and Jalife J, Philadelphia, PA: Elsevier, 2003.
- Rivolta I, Abriel H, Tateyama M, Liu H, Memmi M, Vardas P, Napolitano C, Priori SG, Kass RS. Inherited Brugada and long QT-3 syndrome mutations of a single residue of the cardiac sodium channel confer distinct channel and clinical phenotypes. *J Biol Chem* 276: 30623–30630, 2001.
- Schwartz PJ, Priori SG, Locati EH, Napolitano C, Cantu F, Towbin JA, Keating MT, Hammoude H, Brown AM, Chen LS. Long QT syndrome patients with mutations of the SCN5A and HERG genes have

- differential responses to Na⁺ channel blockade and to increases in heart rate. Implications for gene-specific therapy. *Circulation* 92: 3381–3386, 1995.
37. Schwartz PJ, Priori SG, Napolitano C. The long QT syndrome. In: *Cardiac Electrophysiology: From Cell to Bedside*. 2000.
 38. Schwartz PJ, Priori SG, Spazzolini C, Moss AJ, Vincent GM, Napolitano C, Denjoy I, Guicheney P, Breithardt G, Keating MT, Towbin JA, Beggs AH, Brink P, Wilde AA, Toivonen L, Zareba W, Robinson JL, Timothy KW, Corfield V, Wattanasirichaigoon D, Corbett C, Haverkamp W, Schulze B, Lehmann MH, Schwartz K, Coumel P, Bloise R. Genotype-phenotype correlation in the long-QT syndrome: gene-specific triggers for life-threatening arrhythmias. *Circulation* 103: 89–95, 2001.
 39. Schwartz PJ, Priori SG, Dumaine R, Napolitano C, Antzelevitch C, Stramba-Badiale M, Richard TA, Berti MR, Bloise R. A molecular link between the sudden infant death syndrome and the Long-QT syndrome. *N Engl J Med* 343: 262–267, 2000.
 40. Schwarz JR. The effect of temperature on Na currents in rat myelinated nerve fibres. *Pflügers Arch* 406: 397–404, 1986.
 41. Shampine LF, Reichelt MW. The MATLAB ODE Suite. *SIAM J Scientific Comput* 18: 1–22, 1997.
 42. Shimizu W, Antzelevitch C, Suyama K, Kurita T, Taguchi A, Aihara N, Takaki H, Sunagawa K, Kamakura S. Effect of sodium channel blockers on ST segment, QRS duration, and corrected QT interval in patients with Brugada syndrome. *J Cardiovasc Electrophysiol* 11: 1320–1329, 2000.
 43. Sicouri S, Quist M, Antzelevitch C. Evidence for the presence of M cells in the guinea pig ventricle. *J Cardiovasc Electrophysiol* 7: 503–511, 1996.
 44. Slawsky MT, Castle NA. K⁺ channel blocking actions of flecainide compared with those of propafenone and quinidine in adult rat ventricular myocytes. *J Pharmacol Exp Ther* 269: 66–74, 1994.
 45. ten Tusscher KHWJ, Noble D, Noble PJ, Panfilov AV. A model for human ventricular tissue. *Am J Physiol Heart Circ Physiol* 286: H1573–H1589, 2004.
 46. Tian XL, Yong SL, Wan X, Wu L, Chung MK, Tchou PJ, Rosenbaum DS, Van Wagoner DR, Kirsch GE, Wang Q. Mechanisms by which SCN5A mutation N1325S causes cardiac arrhythmias and sudden death in vivo. *Cardiovasc Res* 61: 256–267, 2004.
 47. Vecchietti S, Rivolta I, Severi S, Napolitano C, Priori S, Cavalcanti S. Computer simulation of wild-type and mutant human cardiac Na⁺ current. *Med Biol Eng Comput* 44: 35–44, 2006.
 48. Viswanathan PC, Rudy Y. Pause induced early afterdepolarizations in the long QT syndrome: a simulation study. *Cardiovasc Res* 42: 530–542, 1999.
 49. Wang DW, Kiyosue T, Sato T, Arita M. Comparison of the effects of class I anti-arrhythmic drugs, cibenzoline, mexiletine and flecainide, on the delayed rectifier K⁺ current of guinea-pig ventricular myocytes. *J Mol Cell Cardiol* 28: 893–903, 1996.
 50. Yan GX, Antzelevitch C. Cellular basis for the Brugada syndrome and other mechanisms of arrhythmogenesis associated with ST-segment elevation. *Circulation* 100: 1660–1666, 1999.

